Novel Inorganic Host Layered Double Hydroxides Intercalated with Guest Organic Inhibitors for Anticorrosion Applications

S. K. Poznyak,[†] J. Tedim,[†] L. M. Rodrigues,[†,‡] A. N. Salak,[†] M. L. Zheludkevich,[*,†] L. F. P. Dick,[‡] and M. G. S. Ferreira[†,§]

Department of Ceramics and Glass Engineering, University of Aveiro, CICECO, 3810-193 Aveiro, Portugal, Rio Grande do Sul Federal University, 90040-06 Porto Alegre, Brazil, and Technical University of Lisbon, IST, ICEMS, Av. Rovisco Pais, 1049-001 Lisbon, Portugal

ABSTRACT Zn−Al and Mg−Al layered double hydroxides (LDHs) loaded with quinaldate and 2-mercaptobenzothiazolate anions were synthesized via anion-exchange reaction. The resulting compounds were characterized by X-ray diffraction, Fourier transform infrared spectroscopy, and scanning electron microscopy/energy-dispersive X-ray spectroscopy. Spectrophotometric measurements demonstrated that the release of organic anions from these LDHs into the bulk solution is triggered by the presence of chloride anions, evidencing the anion-exchange nature of this process. The anticorrosion capabilities of LDHs loaded with organic inhibitors toward the AA2024 aluminum alloy were analyzed by electrochemical impedance spectroscopy. A significant reduction of the corrosion rate is observed when the LDH nanopigments are present in the corrosive media. The mechanism by which the inhibiting anions can be released from the LDHs underlines the versatility of these environmentally friendly structures and their potential application as nanocontainers in self-healing coatings.

KEYWORDS: layered double hydroxides • organic inhibitors • corrosion • nanocontainer • aluminum alloy

INTRODUCTION

The degradation of metallic substrates by corrosion processes is an economic problem of huge proportions: studies show that the direct costs associated with corrosion degradation of metallic structures correspond to 3−4% of the gross domestic product (1).

The most common method for corrosion protection is the application of organic polymer coatings onto metallic substrates. Until recently, chromate-derived pigments were incorporated frequently into these coatings to prevent or at least delay the occurrence of corrosion. However, the use of these inhibitors was prohibited because of the high toxicity of chromium(VI), leading to a demand for systems with comparable protective action but at the same time that are environmentally friendly. One approach that has been undertaken to improve the corrosion protection is the use of technology that provides not only a physical barrier against aggressive species but also a self-healing ability in local sites where corrosion starts during the service life of coated metallic structures.

There are several types of self-healing processes. Some are intended to restore the coating integrity as in the case of healing by polymerization (2, 3); others aim at the blocking of defects (self-sealing) (4, 5). The active corrosion protection can also be envisaged as a healing process in the sense that the degradation of coatings, and consequent loss of the protective action against corrosion, is refrained by the presence of corrosion-inhibiting species. In spite of some species being effective as corrosion inhibitors, their interaction with the coatings can be detrimental, leading to the loss of inhibition capability, coating degradation, or both (6). A possible strategy to overcome this problem is the use of inert "host" systems of nanometer dimensions, referred hereafter as *nanocontainers* or *nanoreservoirs*, loading them with the desired inhibitors. Accordingly, the nanocontainers will store the inhibitors while the coating is able to keep the metallic substrate protected. The release of inhibitors occurs when the coating starts to degrade and the corrosion processes begin (7). The host structures that have been used as nanoreservoirs in corrosion science include cyclodextrins (8, 9), oxide nanoparticles (10, 11) and cation-exchange solids (12).

The layered double hydroxides (LDHs), also known as anionic clays or hydrotalcite-like compounds, are anion-exchange substances consisting of stacks of positively charged, mixed-metal hydroxide layers between which anionic species and solvent molecules are intercalated (13). The most common LDHs can be represented by the general formula $[M^{2+}_{1-x}M^{3+}_x(OH)_2]A^{n-}_{x/n} \cdot mH_2O$. Their structure is derived from brucite, $[Mg(OH)_2]$, in which some divalent metal cations M^{2+} (Mg^{2+}, Zn^{2+}, Fe^{2+}, Co^{2+}, Cu^{2+}, and others) are replaced by trivalent cations M^{3+} (Al^{3+}, Cr^{3+}, Fe^{3+}, Ga^{3+}, and others). This generates a positive charge that is com-

pensated for by the presence of anions A^{n-} between the hydroxide layers. The LDHs have been applied as catalysts and catalyst supports (14), polymer stabilizers (15, 16), and traps of anionic pollutants (17). In addition, they have been considered for the delivery of drugs at the cellular level, with several studies showing their low toxicity and high biocompatibility, together with the ability to control the release of active species under certain circumstances (18−20). Therefore, the nanostructured systems used for drug-delivery purposes are prospective systems for the incorporation/encapsulation of corrosion inhibitors.

The application of hydrotalcite-like compounds in corrosion science has covered different aspects. In some studies, the LDHs have been produced in situ, on the top of metallic substrates as protective films (12, 21−26). Hydrotalcite-based conversion films have demonstrated good corrosion protection, and some research groups have been trying to improve the interaction between these conversion films and organic coatings (27, 28). A different perspective is to use these anionic clays as containers for corrosion inhibitors and incorporate them into the organic coatings. In this case, the aims are two-fold: not only to release the species that impart *active* protection but also to trap the corrosive agents (Cl^-, SO_4^{2-}). Regarding this topic, several works by Buchheit et al. (29, 30), Williams and McMurray (31−33) and others (34−36) can be found in the literature.

Within the LDH family, a class of materials with emerging importance is that constituted by the LDHs loaded with organic anions (37, 38). Two short studies on these materials are available in the literature. Williams and McMurray (31) prepared LDHs with different organic species (benzotriazole, ethyl xantate, and oxalate) by rehydration of commercial hydroltalcite [$Mg_6Al_2(OH)_{16} \cdot CO_3 \cdot 4H_2O$]. The resulting layered systems were inserted into a poly(vinylbutyral) coating, prepared by a bar cast on the top of AA2024-T3. The filiform corrosion studies showed that benzotriazole is a very efficient anion, but not as efficient as CrO_4^{2-}. In another report, Kendig and Hon (34) prepared LDHs intercalated with 2,5-dimercapto-1,3,4-thiadiazolate in a similar way and studied the inhibiting properties of this anion with respect to the oxygen reduction reaction on copper.

In this paper, we describe the synthesis and characterization of new Zn−Al and Mg−Al LDHs intercalated with quinaldate (QA) and 2-mercaptobenzothiazolate (MBT) organic anions. Mercaptobenzothiazole has been recognized as an effective corrosion inhibitor for different metal substrates (39, 40). Moreover, this organic inhibitor has already been encapsulated within other types of nanocontainers to provide long-term protection. In particular, Khramov and colleagues have found that sol−gel coatings doped with 2-mercaptobenzothiazole/β-cyclodextrin inclusion complexes show better corrosion protection properties when compared to the same coatings without the nanocontainers (9). More recently, our group has studied the incorporation of this azole inhibitor into halloysite nanotubes coated with polyelectrolyte shell multilayers. The hybrid sol−gel films doped with these nanomaterials imparted a long-term, enhanced

corrosion protection with respect to the undoped film (41). Conversely, the study of the inhibiting effect of quinaldic acid is recent. Our group showed that quinaldic acid provides a remarkable active protection against corrosion of AA2024 (42).

The present study is divided into three main sections. First, the synthesized LDHs are structurally and morphologically characterized by X-ray diffraction (XRD), Fourier transform infrared spectroscopy (FTIR), and scanning electron microscopy (SEM). Then, the mechanisms associated with the release of the inhibitor are investigated by spectrophotometry and interpreted considering the structural information provided by XRD. Finally, the anticorrosion activity of these pigments with respect to bare AA2024 is electrochemically assessed by electrochemical impedance spectroscopy (EIS). The aim is not only to develop nanocontainers for active corrosion protection but also to rationalize the level of anticorrosion efficiency in terms of (i) the structural parameters and (ii) the release and inhibition mechanisms.

MATERIALS AND METHODS

Chemicals. All of the chemicals were obtained from Aldrich, Fluka, and Riedel-de Häen, with ≥98 % of ground substance, and used as received.

Synthesis of LDHs Intercalated with Organic Inhibiting Anions. There are two main approaches to the preparation of LDHs with the required structure and composition: (i) anion-exchange reaction using a precursor LDH and (ii) direct synthesis by coprecipitation (13). The first approach was adopted in the present work for the preparation of organic-intercalated LDHs in order to avoid the formation of insoluble salts of metal cations with the organic anions, which can occur in the case of direct precipitation synthesis. The synthesis was carried out under an argon atmosphere, and all of the solutions were prepared using boiled distilled water to avoid contamination with carbonate. Otherwise, this anion is readily incorporated and tenaciously held in the LDH interlayer galleries, causing a loss of the anion-exchange ability. The preparation of the anionic clays is divided into two main steps: (i) the synthesis of LDH precursors and (ii) the ion-exchange reaction with substitution of the inorganic anions by inhibiting organic anions.

The $M^{2+}:M^{3+}$ ratio chosen for the synthesis of the LDH precursors in the present work was 2:1 to obtain stable layered compounds. The Mg(2)−Al and Zn(2)−Al LDHs intercalated with nitrate anions were first prepared because the single-charged nitrate anions can be easily displaced from the interlayer galleries by other anions (13), and hence they are suitable for the following anion-exchange step. For this purpose, 50 mL of a solution containing 0.5 M (NO_3)$_2 \cdot 6H_2O$ (M = Mg and Zn) and 0.25 M $Al(NO_3)_3 \cdot 9H_2O$ was slowly added to 100 mL of a 1.5 M $NaNO_3$ solution (pH = 10) under vigorous stirring at room temperature (the addition took approximately 1.5 h). During this reaction, the pH of the solution was kept constant (pH = 10 ± 0.5) by the simultaneous addition of a 2 M NaOH solution. Then, the obtained slurry was subjected to hydrothermal treatment at 65 °C for 24 h for crystallization of the LDHs. Afterward, the product was centrifuged and washed four times with boiled distilled water. A small fraction of the LDHs was dried at 50 °C for analysis, while the rest of it was used in the anion-exchange reaction for the replacement of nitrate by quinaldate (QA) or 2-mercaptobenzothiazolate (MBT).

The anion-exchange reaction was carried out by dispersing the precursor LDH in an aqueous solution containing the organic anions in double excess. Sodium salts of quinaldic acid and MBT were previously prepared by neutralization of the aqueous

solutions of quinaldic acid and MBT with equivalent amounts of NaOH. Subsequently, the white gel-like LDH precursors were dispersed in a solution of 0.1 M NaQA (pH ≈ 7) or 0.1 M NaMBT (pH ≈ 10) under an argon atmosphere. The total amount of this solution (120 mL) was split into two portions of 60 mL. The LDH precursors were added to one of these portions followed by centrifugation. This procedure was repeated with the second portion of the organic anion solution. Finally, the organic anion-loaded LDH powders were washed four times with boiled distilled water, frozen, and then dried by lyophilization at −78 °C.

Characterization of LDH Powders. The structure of the LDH powders was studied by X-ray diffraction (XRD; Philips X'Pert diffractometer, Cu Kα radiation) and Fourier transform infrared spectroscopy (FTIR; Bruker Equinox IFS 55 spectrophotometer). The particle morphology and composition were characterized by scanning electron microscopy/energy-dispersive X-ray spectroscopy (SEM/EDS; Hitachi S-4100 microscope with an electron beam energy of 25 kV and a beam current of 10 μA).

Study of the Anion-Exchange Mechanism by Spectrophotometry. The concentration of organic anions released from the LDHs to solution was measured photometrically using a Shimadzu UV-3100 spectrophotometer. The absorption spectra of QA and MBT anions show several pH-sensitive peaks within the spectral region 220−400 nm. The calibration was performed at a defined pH of the solution: pH = 4 for QA and pH = 8 for MBT, using the absorption peaks at $\lambda = 319$ nm (QA) and $\lambda = 312$ nm (MBT). To study the kinetics of anion release from the nanoreservoirs, 50 mg of the LDH powder was added to 10 mL of a NaCl solution under stirring. The suspensions were centrifuged at definite time intervals, and very small aliquots were taken for analysis. Then, the LDHs were again stirred to continue the anion release process.

Assessment of the Anticorrosion Protection of AA2024 by LDHs. The protection efficiency of the LDHs was investigated using the electrochemical impedance spectroscopy (EIS) technique on a bare AA2024 aluminum alloy for 2 weeks. The EIS measurements were carried out at room temperature in a three-electrode cell consisting of a saturated calomel reference electrode, a platinum foil counter electrode, and the AA2024 sample as a working electrode in the horizontal position (exposed area of ca. 3 cm²). The cell was placed in a Faraday cage to avoid interference of the external electromagnetic fields. The electrolyte was a 0.05 M NaCl aqueous solution (10 mL), quiescent and in equilibrium with air. The EIS measurements were performed using a Gamry FAS2 femtostat with a PCI4 controller. The selected frequency range was from 5×10^4 to 7×10^{-3} Hz with a step of 7 points per decade and 10 mV of amplitude. All of the spectra were recorded at open-circuit potential. The impedance plots were fitted using different equivalent circuits with the Elchem Analyst software package from Gamry.

Prior to measurements, the AA2024 substrates were cleaned and etched according to standard commercial procedures: alkaline cleaning in Metaclean T2001 at 68 °C for 25 min, alkaline etching in Turco Liquid Aluminetch N2 at 60 °C for 45 s, and acid etching in Turco Liquid Smutgo NC at 30 °C for 7 min each, followed by washing with distilled water.

The AA2024 samples were placed in contact with LDH suspensions in a 0.05 M NaCl solution (50 mg of LDHs per 10 mL of solution). After the corrosion tests, optical photographs of the metal substrates were taken for visual control of the corrosion processes. The inhibiting properties of MBT and QA were also studied in a 0.05 M NaCl solution, in the absence of LDHs, at different pHs.

RESULTS AND DISCUSSION

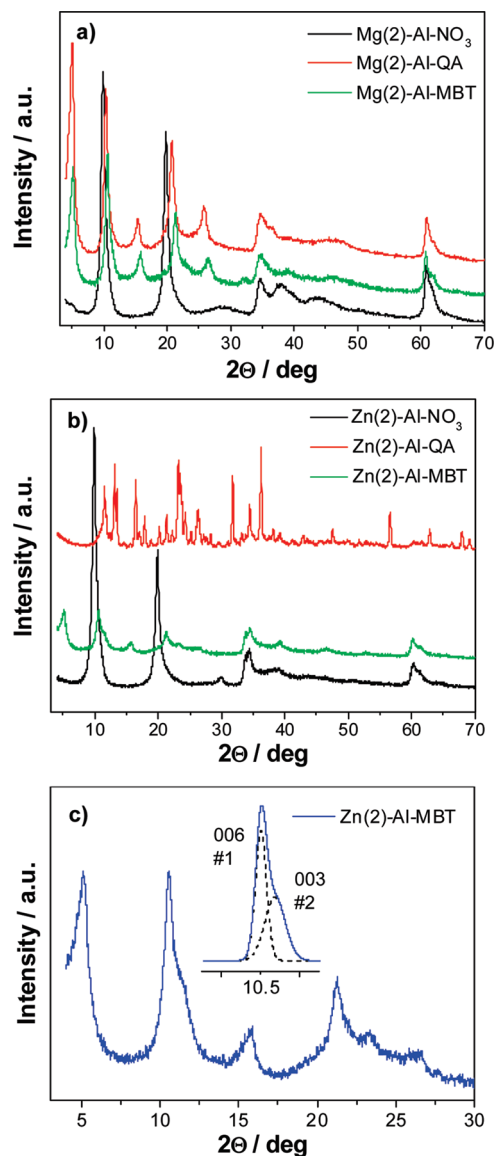**Characterization of LDH Powders.** The XRD patterns for nitrate-loaded Mg(2)−Al and Zn(2)−Al LDHs (Figure

FIGURE 1. XRD patterns of Mg(2)−Al (a) and Zn(2)−Al (b) LDHs intercalated with NO₃⁻, QA, and MBT anions. (c) XRD pattern of Zn(2)−Al−MBT at the region of (00*l***) fundamental reflections.**

1) show sharp basal (00*l*) reflections at low 2θ angles corresponding to diffraction by hydroxide layers. The basal spacing can be estimated from the *d*(003) position using Bragg's law, which gives 0.891 nm for Mg(2)−Al−NO₃ and 0.889 nm for Zn(2)−Al−NO₃. The values obtained are in good agreement with the literature data (43). Moreover, the peaks in the diffractograms correspond to a single-phase LDH structure, demonstrating the good quality of the materials synthesized. Nonetheless, if the Zn:Al ratio was increased up to 3, additional peaks assigned to the ZnO phase would be present in the diffractogram.

Analysis of the XRD patterns of both the MBT- and QA-containing LDHs reveals that the diffractograms are rather different with respect to the nitrate-containing LDHs Mg(2)−Al−NO₃ and Zn(2)−Al−NO₃. Initially, several attempts to describe the organic-substituted compositions as single-phase LDHs were made, including a phase analysis with different polytypes of hydrotalcite-like structure (44, 45),
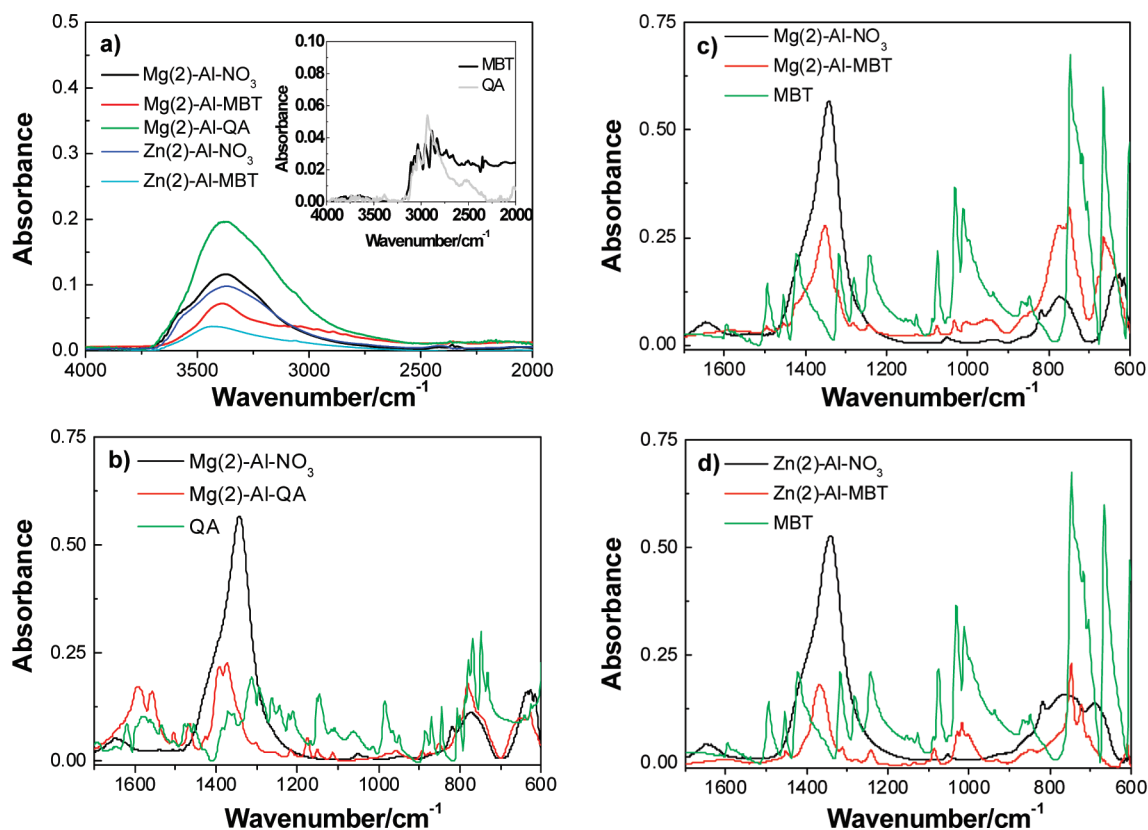
FIGURE 2. FTIR spectra of Mg(2)−Al and Zn(2)−Al LDHs intercalated with NO_3^-, QA, and MBT anions, superposed with spectra of pure MBT and QA powders.

which were unsuccessful. A closer examination of the XRD patterns for these organic-substituted systems revealed a broadening and splitting of some fundamental LDH reflections of (00*l*) type. For instance, the asymmetric broad peak in the vicinity of $2\theta = 10.3-10.6°$ is here assigned to the (006) reflection of phase #1 overlapped with the (003) reflection of phase #2 (see the inset in Figure 1c). As a consequence, the most intense diffraction lines correspond to LDH phases with different interlayer distances.

A description of the corresponding XRD patterns is acceptable if one assumes that the two LDH-type phases are present in both LDH−MBT and LDH−QA. In this sense, the basal spacings *d*(003) associated with these phases were estimated to be 1.70, 1.74, and 1.72 nm (phase #1) and 0.83, 0.85, and 0.82 nm (phase #2) for Mg(2)−Al− MBT, Mg(2)−Al−QA, and Zn(2)−Al−MBT, respectively. These results suggest that the organic guest anions assume two particular orientations within the interlayer galleries. Similar phenomena were reported to occur naturally in the LDHs intercalated with big organic molecules (13, 46).

The XRD pattern obtained for Zn(2)−Al−NO_3 after anion-exchange reaction with QA is quite different when compared to that of the precursor Zn(2)−Al−NO_3. More specifically, the diffractogram of Zn(2)−Al−QA shows a multiphase structure, possibly consisting of a mixture of zinc and aluminum hydroxides and insoluble salts of QA, without any peaks typical of the LDH structure.

The FTIR spectra of the LDHs and pure organic inhibitor powders are shown in Figure 2. All of the LDH samples show broad bands in the range of 3200−3700 cm^{-1} due to the stretching mode of structural OH groups in the metal hydroxide layer (panel a), which are not present in the pure QA and MBT.

In the case of nitrate-loaded LDHs, a peak occurring at 1650 cm^{-1} can be ascribed to the bending mode of interlayer water molecules. Additionally, an intensive peak occurring at ca. 1350 cm^{-1}, superposed with a shoulder near 1400 cm^{-1}, corresponds to symmetric and asymmetric stretching modes of nitrate. The broad peaks below 1000 cm^{-1} can be assigned to M^{2+}−OH or Al^{3+}−OH stretching modes. Following the exchange of NO_3^- by QA anions (panel b), the peak at 1348 cm^{-1} significantly decreases and several new peaks appear in the corresponding FTIR spectrum. A comparison between the FTIR spectra of Mg(2)−Al−QA and pure QA allows one to conclude that these new peaks can be assigned to different vibration modes of intercalated QA anions. Furthermore, variation of the peak positions and intensities may be indicative of the interaction between the intercalated organic anions and the positively charged hydroxide layers. The same trend was found for LDHs loaded with MBT (panels c and d).

These results clearly indicate the successful and rather complete ion exchange of nitrate anions by inhibiting organic anions, leading to the creation of new nanocontainers for organic inhibitors.

The results of SEM analysis for Mg(2)−Al and Zn(2)−Al LDH powders are depicted in Figure 3. Generically, all of the powders are aggregates of smaller particles with a
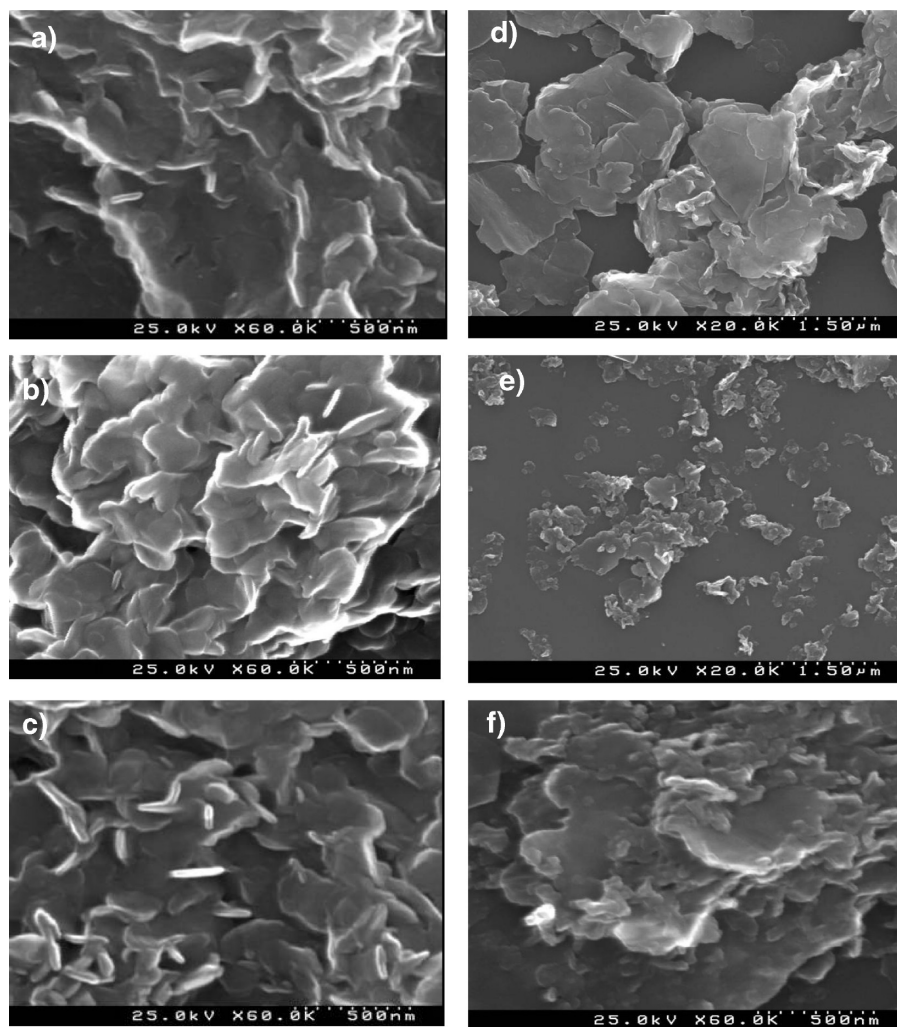
FIGURE 3. SEM micrographs of (a) Mg(2)–Al–NO₃, (b) Mg(2)–Al–QA, (c) Mg(2)–Al–MBT, (d) Zn(2)–Al–NO₃, and (e and f) Zn(2)–Al–MBT particles.

Table 1. EDS Analysis of the LDH Nanocontainers

	atomic % ratio					
	Mg:Al		Zn:Al		Al:S	
sample	theoretical	experimental	theoretical	experimental	theoretical	experimental
Mg(2)–Al–QA	2:1	1.9:1				
Mg(2)–Al–MBT	2:1	2.0:1			1:1	0.8:1
Zn(2)–Al–MBT			2:1	1.9:1	1:1	0.6:1

platelike morphology. It seems, though, that this morphology is rather different, depending on the composition of the hydroxide layers. More specifically, Zn–Al systems show larger sizes of aggregates (panels d–f) when compared to Mg–Al systems (panels a–c). Following anion exchange, the morphology of LDH materials does not change appreciably.

The EDS technique was used here to assess the atomic composition of the obtained powders. The corresponding results are presented in Table 1. Two main aspects can be highlighted. First, the $M^{2+}:M^{3+}$ ratio is in agreement with the expectations considering the proportion of metal salt precursors used in the synthesis (2:1). Second, the intercalation of the MBT anions is proved to have occurred because they are the only available source of sulfur.

Kinetics of Organic Anion Release from LDH Pigments. As mentioned previously, the LDHs are anion-exchange compounds, so the organic inhibiting anions can be exchanged by "aggressive" inorganic ions, such as chlorides present in the environment. Thus, these anions can work as a trigger for the release of the inhibitor on demand. On the other hand, the exchange reaction is an "extra" feature from the corrosion protection point of view because it may also contribute to the decrease of the local corrosion rate by the entrapment of aggressive anions in the LDH galleries, thereby reducing the aggressiveness of the environment. Therefore, the LDHs can be envisaged as both containers and traps, and the under-
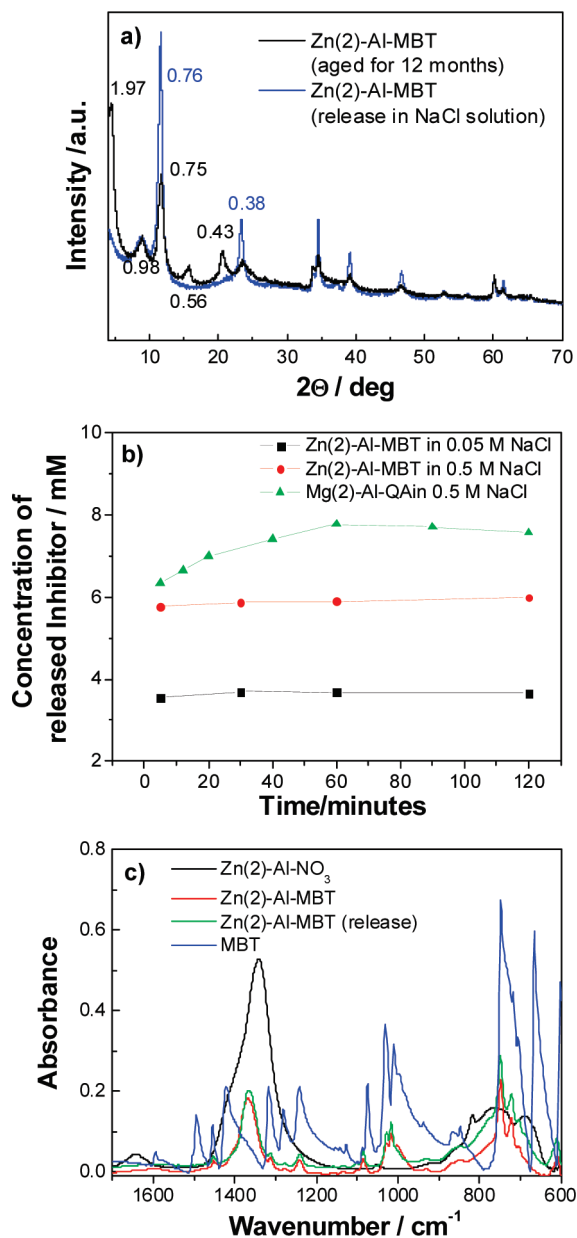
FIGURE 4. (a) XRD patterns of Zn(2)−Al−MBT before and after the release of MBT in 0.05 M NaCl. (b) Concentration vs time plots for Mg(2)−Al−QA and Zn(2)−Al−MBT LDHs in 0.05 and 0.5 M NaCl solutions. (c) FTIR spectra.

standing of the exchange mechanism assumes a vital importance.

Before experiments were performed on the organic anion release, the LDH compositions were tested with respect to their stability upon storage. The stability of the nanocontainers is extremely important from the standpoint of industrial applicability. Analysis of the diffractograms before (Figure 1b) and after aging (Figure 4a) reveals that the structural parameters of coexisting LDH phases are not constant over time. The aged Zn(2)−Al−MBT powder showed an increase in the d spacing for phase #1 (from 1.72 to 1.97 nm) and a decrease for phase #2 (from 0.82 to 0.75 nm). This effect may be due to the structural arrangements of the intercalated anions in the galleries, possibly induced by a change in the hydration degree. It should also be noted that

this process seems to be accompanied by some decomposition of one of the LDH phases, with the appearance of a small diffraction peak at the characteristic d spacing ≈ 0.98 nm ($2\theta \approx 9°$) in the XRD pattern of the aged Zn(2)−Al−MBT sample, which belongs neither to phase #1 nor #2. At the same time, any traces of pure MBT could not be detected.

Figure 4a shows the XRD patterns of aged Zn(2)−Al−MBT before and after dispersion in a 0.05 M NaCl solution for 24 h. The differences observed in the XRD patterns indicate a considerable change in the phase content. The release of MBT is thought to occur mainly from phase #1. Moreover, the MBT−Cl exchange process seems to promote a reorientation of the remnant MBT anions, thereby inducing a transition from phase #1 to phase #2, with the former becoming negligible. The relative instability of the LDH phase with a large interlayer distance (phase #1) looks natural because the electrostatic interactions in such a solid are certainly lower. The appearance of a new LDH phase, Zn(2)−Al−Cl, with $d(003)$ at 0.76 nm (43) can be detected in the XRD pattern by a significant increase in the intensity of the corresponding diffraction peak, although it must be stressed that Zn(2)−Al−Cl and phase #2 of Zn(2)−Al−MBT are practically indistinguishable by XRD.

The ion exchange was proven qualitatively by XRD as described above. Quantitatively, the kinetics of anion exchange was monitored by spectrophotometry. Figure 4b presents the evolution of the MBT and QA concentrations during immersion of the LDH powders in a 0.05 M NaCl solution. The release of MBT and QA from LDHs proceeds very rapidly (during the first several minutes); after 1 h, there is no significant variation in the anion concentration because chemical ion-exchange equilibrium is attained. The increase in the NaCl concentration up to 0.5 M intensifies the release and confirms the chemical nature of this anion-exchange process, governed by a dynamic equilibrium and exchange isotherm. Figure 4c shows the FTIR spectrum of Zn(2)−Al−MBT after release of MBT in a 0.05 M NaCl solution. There are no significant changes in the spectrum when MBT is released into the solution, showing that, in spite of some MBT being released, a considerable amount of this anion is still within the LDH nanocontainers with respect to the ion-exchange equilibrium constant.

Anticorrosion Capabilities of LDHs Intercalated with Inhibiting Organic Anions. The LDHs loaded with inhibiting organic anions were tested as possible anticorrosion pigments using EIS. Figure 5 shows the Bode plots obtained for AA2024 in contact with different LDH-containing solutions (panels b−f) during the first week of immersion in a NaCl solution. The impedance spectra recorded for an AA2024 electrode in contact with a 0.05 M NaCl solution (with no LDHs) were also recorded at similar times for comparison purposes (panel a). After 1 h of immersion, two well-defined time constants are observed on the Bode plots for the electrode immersed in a NaCl solution without LDHs; these relaxation processes are associated with the response from the oxide film (at the middle of the selected frequency range) and the occurrence of corrosion processes (low
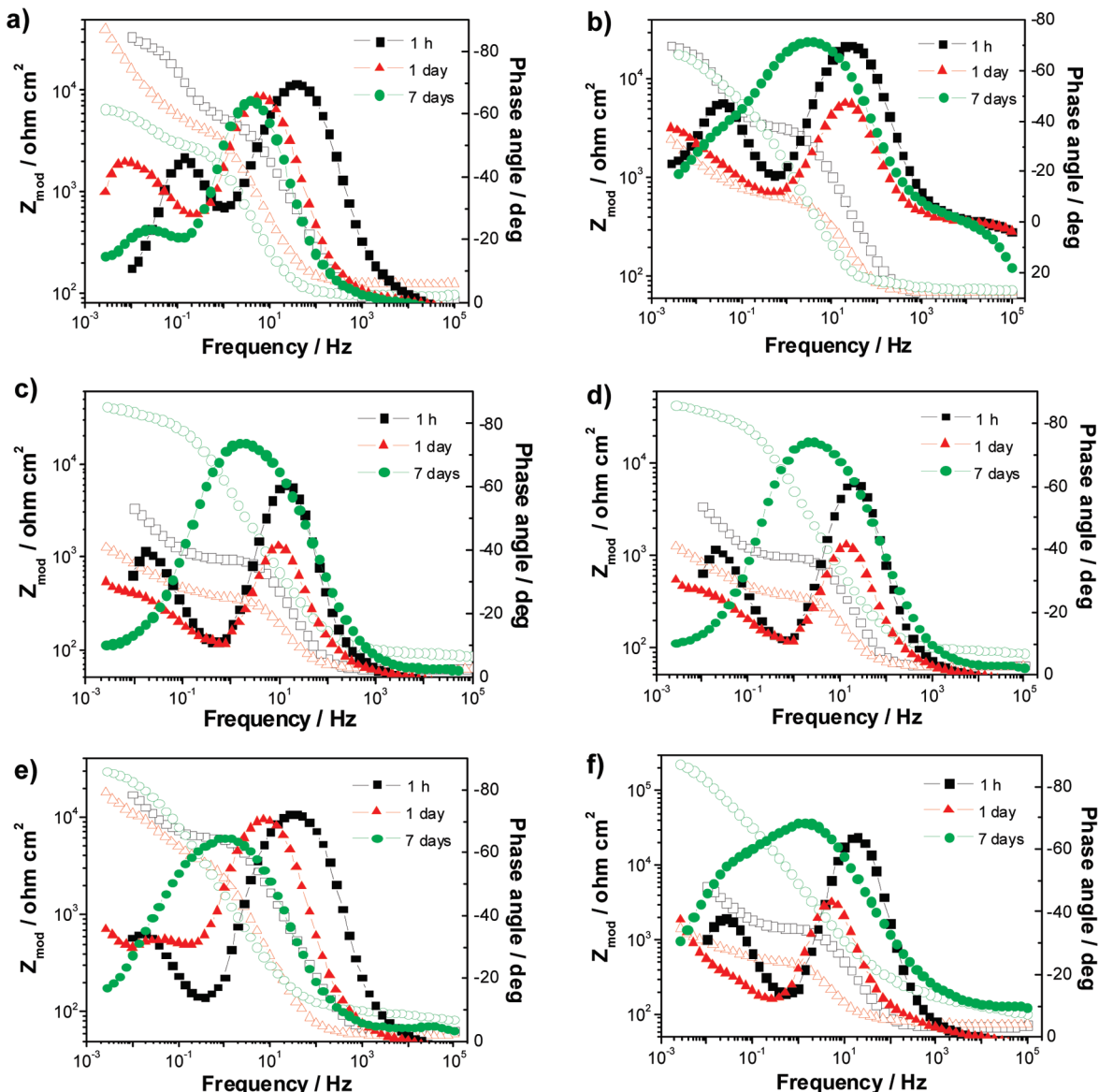
FIGURE 5. Bode plots of the impedance measured on bare AA2024 in (a) 0.05 M NaCl, (b) Mg(2)—Al—NO₃ + 0.05 M NaCl, (c) Mg(2)—Al—QA + 0.05 M NaCl, (d) Mg(2)—Al—MBT + 0.05 M NaCl, (e) Zn(2)—Al—NO₃ + 0.05 M NaCl, and (f) Zn(2)—Al—MBT + 0.05 M NaCl.

frequencies). Additionally, the impedance module values decrease as a function of time (1 h vs 24 h), indicating degradation of the metallic surface. However, the two time constants observed for 1 and 7 days of immersion are associated with different processes. The relaxation process due to the presence of the oxide film disappears because of its degradation and the beginning of pitting corrosion attack. Hence, the two time constants can be assigned to the corrosion process. Namely, the high-frequency time constant is related to the capacitance of the electrochemical double layer and polarization resistance, whereas the low-frequency relaxation process is associated with diffusion. The diffusion limitations can appear because of the formation of corrosion product deposits on the metal surface, which limits the transport of reactants and soluble corrosion products between the metal surface and the bulk solution. This is evident in Figure 6a, where a thick film of corrosion products covering the electrode can be observed.

The impedance spectra do not change to a great extent at the beginning of immersion when nitrate-containing LDHs are dispersed in solution. Both time constants associated with corrosion and film oxide formation can still be detected. The impedance values after 1 h of immersion are even lower for solutions with nitrate-loaded LDHs than those for the solution without these LDHs (cf. panels a, b, and e). Nevertheless, the results differ as the immersion time increases. For Mg(2)—Al—NO₃, the impedance decreases 10 times after 24 h, but 1 week later, the impedance increases back to the initial magnitude. This is attributed to the increase in the polarization resistance and consequent reduction of the corrosion rate. Conversely, for Zn(2)—Al—NO₃, the impedance remains more or less constant over 1 week. These results suggest some additional positive effects of Zn²⁺ on the corrosion protection of the aluminum alloy. In fact, there are some studies reporting that Zn²⁺ cations are released from LDHs into solution, either from the interlayer galleries
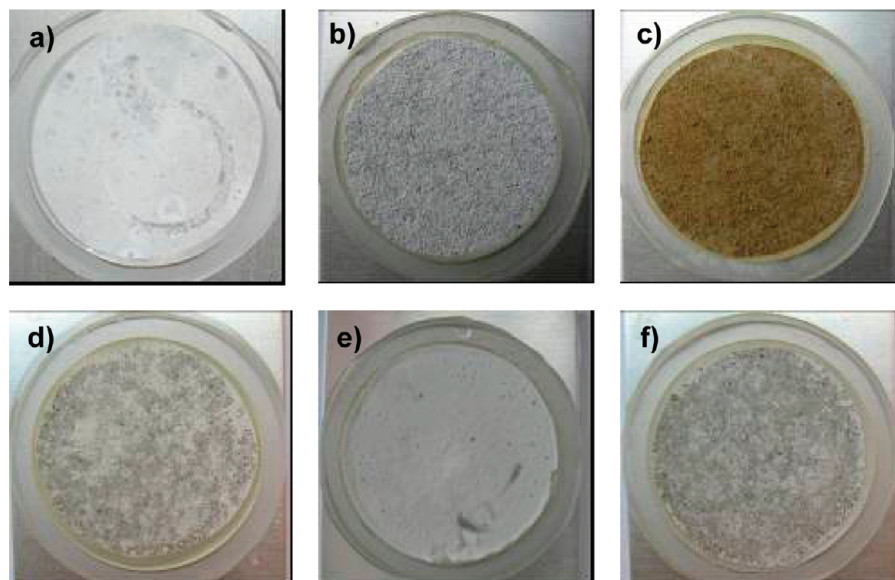
FIGURE 6. Optical micrographs of AA2024 samples after corrosion tests for 14 days in (a) 0.05 M NaCl, (b) Mg(2)−Al−No$_3$ + 0.05 M NaCl, (c) Mg(2)−Al−QA + 0.05 M NaCl, (d) Mg(2)−Al−MBT + 0.05 M NaCl, (e) Zn(2)−Al−NO$_3$ + 0.05 M NaCl, and (f) Zn(2)−Al−MBT + 0.05 M NaCl.

or from the metal hydroxide layers as a result of structural arrangements, showing some inhibition effect (29). A similar trend can be found here upon analysis of the Bode plots for the LDHs loaded with organic inhibitors, with the Zn(2)−Al LDH system (panel f) revealing better corrosion protection capabilities than the Mg(2)−Al LDHs (panels c and d).

In the case of LDHs with QA and MBT anions during the first day of immersion, the impedance is even lower than that in a pure NaCl solution (see Figure 5, panels c, d, and f). Notwithstanding these initial observations, the impedance sufficiently increased after longer immersion times. In the case of QA-loaded LDHs, the impedance remains lower [Mg(2)−Al−QA, panel c] with respect to that in a pure NaCl solution, whereas the MBT-loaded LDHs show significantly improved corrosion protection. This is more evident for the electrode in contact with the Zn(2)−Al−MBT-containing solution (panel f), whose impedance is about 10 times higher in comparison with that in a pure NaCl solution and may be due to the formation of a rather compact protecting film on the AA2024 surface. This suggestion is supported by the visual observations of the samples after the immersion corrosion tests.

Figure 6 depicts optical photographs of AA2024 samples after 2 weeks of immersion. All of the samples exhibit thick layers of deposits. Nevertheless, the compactness and color of these layers depend strongly on the solution composition. For example, in the case of QA-loaded LDHs, the color is brown. EDS analysis of these deposits (not shown) confirms the presence of LDH particles. In the case of the aluminum alloy immersed in the electrolyte with MBT-containing LDHs, the structures of the corrosion products are different. A denser and more compact protective film is formed on the aluminum alloy surface in comparison with the other LDHs. Thus, the MBT released from LDHs provides a more effective long-term protection against corrosion of AA2024, and the LDHs can be considered as potential nanocontainers to be used in protective coatings.

Study of the Inhibiting Effect of Organic Anions Used for Intercalation in LDHs. To understand the mechanism of corrosion inhibition conferred by QA- and MBT-loaded LDHs on AA2024, the effects of QA and MBT were also investigated under different conditions. More specifically, the pH is one of the most important factors that can significantly influence the inhibiting properties of different compounds, so a detailed study of this effect is presented here.

Figure 7 presents the EIS spectra obtained for AA2024 in contact with several 0.05 M NaCl solutions, containing MBT and QA anions at different pHs. The pH of the solution exerts a strong influence on the corrosion-inhibiting activity of both inhibitors. The best anticorrosion effect was found for neutral solutions with MBT and QA inhibitors. Lowering or increasing the pH leads to a significant decrease of their protective action. It is important to note that the increase in the QA concentration from 20 to 50 mM (pH constant, Figure 7b) results in a deterioration of inhibition, probably because of the intensification of the QA complexing activity. Certainly, this shifts the reaction equilibrium toward metal dissolution. These results explain the detrimental effect of the LDHs with QA anions on the corrosion of AA2024 observed above.

The influence of the LDH matrix on the anticorrosion activity of the organic inhibitors was also investigated (Figure 8). In these experiments, a specific amount of Zn(2)−Al−MBT LDH (50 mg per 10 mL) was added to a 0.05 M NaCl solution. The suspension was stirred for 1 h to reach equilibrium (recall Figure 4) and then centrifuged to remove nonsoluble LDH particles. The concentration of MBT in the supernatant solution was determined spectrophotometrically and found to be ca. 2.5 mM; the pH of the solution was 8. A 2.5 mM NaMBT/0.05 M NaCl solution (pH = 8) was prepared by dissolution of NaMBT and used for comparison purposes.
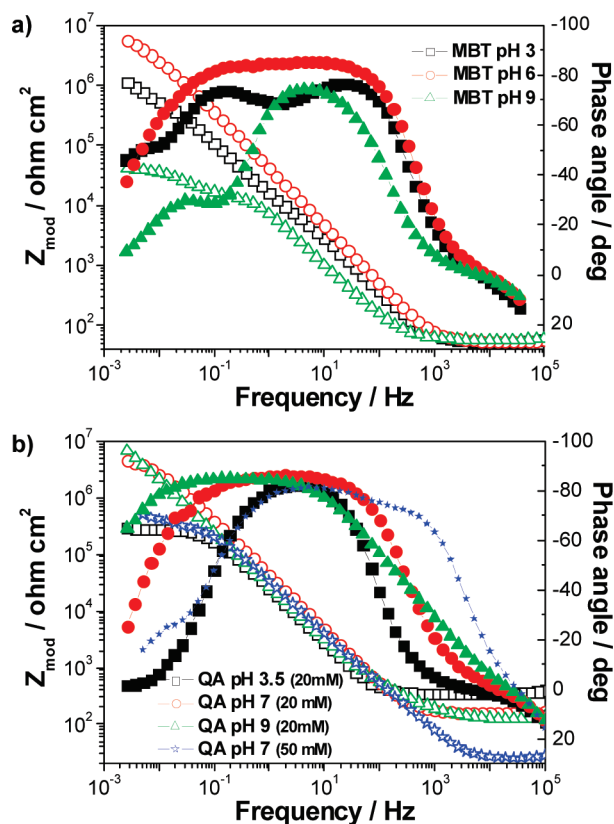
FIGURE 7. Bode plots of the impedance measured on bare AA2024 after 1 week of immersion in (a) 0.45 mM MBT + 0.05 M NaCl (pH = 3, 6, and 9) and (b) 0.02 M NaQA + 0.05 M NaCl (pH = 3.5, 7, and 9) and 0.05 M NaQA + 0.05 M NaCl (pH = 7).
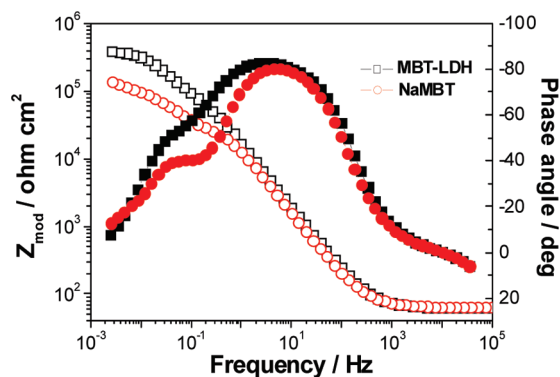

FIGURE 8. Bode plots of the impedance measured on bare AA2024 after 1 day of immersion in 2.5 mM NaMBT + 0.05 M NaCl solution (pH = 8) prepared by the release of MBT^- from $Zn(2)-Al-MBT$ and 2.5 mM NaMBT + 0.05 M NaCl (pH = 8) prepared from a NaMBT reagent.

The UV–vis spectra of both solutions were found to be similar (not shown here).

The solution of MBT released from the LDHs denotes better anticorrosion activity when compared to the NaMBT solution with identical anion concentration and pH. This is more evident after 1 day of testing. Moreover, one can find additional considerations on the influence of the Zn–Al–LDH structure by comparing the Bode plots of Figure 5f (LDHs present) and Figure 8 (LDHs absent). For small immersion times, the presence of LDHs seems to be detrimental, while the opposite effect seems to occur for longer periods. This can be explained considering the processes that occur in the course of time. The AA2024 surface shows active sites with respect to corrosion (intermetallic S phases) that in aggressive media begin to corrode. At this stage, the pH of the solution has a strong effect on the inhibiting properties of MBT (recall Figure 7a) and the LDH particles may produce high local concentrations of hydroxyl ions near the aluminum surface, thereby activating the intermetallics and additionally decreasing the anticorrosion effect of the released MBT. As the time follows, MBT forms a multilayer protective film on AA2024, and this seems to be favored in the presence of LDHs. In other words, the sedimentation of LDH powders onto metal surfaces seems to have a negative effect on the protection because of the local increase in the pH, but the released inhibiting ions positively contribute to the corrosion resistance. The net result of these opposite effects will ultimately determine the final action of the pigment. Although, it must be stressed that the detrimental effect arising from the local alkalization of the metal substrate in the presence of LDHs can be neglected when these layered compounds will be used (or dispersed) as pigments in protective coatings or when the corrosive medium will be acidified.

CONCLUSIONS

New LDHs intercalated with two different organic inhibitor anions were synthesized for the first time. The anion-exchange reaction of nitrate-loaded LDH precursors was used to create the containers of organic inhibitors. The compounds obtained are nanocrystalline with a platelike morphology. More importantly, the present work has undoubtedly shown that the release of inhibiting anions from the LDHs is governed by dynamic equilibrium. The leaching of an inhibitor occurs by an exchange mechanism (release of an inhibitor and entrapment of aggressive chlorides) and the release of an inhibitor is sequential, providing *protection on demand*.

Electrochemical studies showed a small anticorrosion activity of these systems with respect to bare AA2024 in neutral sodium chloride solutions for small immersion times (less than 24 h). This effect may be explained by a local alkalization of the solution in the presence of hydroxide-rich LDH particles, which decreases the corrosion-inhibiting activity of MBT and QA. However, for longer immersion times, the corrosion processes are efficiently inhibited because of the formation of a protective film, with the MBT-loaded LDHs revealing a better performance than the QA-loaded ones.

The LDHs are versatile structures with the potential ability to incorporate different organic or inorganic anions. These materials are worthy of further investigation as inhibiting nanomaterials for AA2024 as well as for other metallic alloys. They can be incorporated into organic coatings in order to assess their potential as nanocontainers for self-healing protection.

REFERENCES AND NOTES

(1) Kruger, J. In *Uhlig's Corrosion Handbook*, 2nd ed.; Revie, R. W., Ed.; Wiley: New York, 2000.

(2) Brown, E. N.; White, S. R.; Sottos, N. R. *J. Mater. Sci.* **2004**, *39*, 1703–1710.

(3) Allsop, N. A.; Bowditch, M. R.; Glass, N. F. C.; Harris, A. E.; O'Gara, P. M. *Thermochim. Acta* **1998**, *315*, 67–75.

(4) Sugama, T.; Gawlik, K. *Mater. Lett.* **2003**, *57*, 4282–4290.

(5) Hikasa, A.; Sekino, T.; Hayashi, Y.; Rajagopalan, R.; Niihara, K. *Mater. Res. Innov.* **2004**, *8*, 84–88.

(6) Shchukin, D. G.; Zheludkevich, M.; Yasakau, K.; Lamaka, S.; Ferreira, M. G. S.; Möwald, H. *Adv. Mater.* **2006**, *18*, 1672–1678.

(7) Shchukin, D. G.; Zheludkevich, M.; Möwald, H. *J. Mater. Chem.* **2006**, *16*, 4561–4566.

(8) Khramov, A. N.; Voevodin, N. N.; Balbyshev, V. N.; Mantz, R. A. *Thin Solid Films* **2005**, *483*, 191–196.

(9) Khramov, A. N.; Voevodin, N. N.; Balbyshev, V. N.; Donley, M. S. *Thin Solid Films* **2004**, *447–448*, 549–557.

(10) Zheludkevich, M. L.; Serra, R.; Montemor, M. F.; Yasakau, K. A.; Salvado, I. M. M.; Ferreira, M. G. S. *Electrochim. Acta* **2005**, *51*, 208–217.

(11) Zheludkevich, M. L.; Serra, R.; Montemor, M. F.; Ferreira, M. G. S. *Electrochem. Commun.* **2005**, *7*, 836–840.

(12) Buchheit, R. G.; Mamidipally, S. B.; Schmutz, P.; Guan, H. *Corrosion* **2002**, *58*, 3–14.

(13) Newman, S. P.; Jones, W. *New J. Chem.* **1998**, *22*, 105–115.

(14) Albertazzi, S.; Basile, F.; Vaccari, A. In *Clay Surfaces: Fundamentals and Applications*; Wypych, F., Satyanarayana, K. G., Eds.; Elsevier: Amsterdam, The Netherlands, 2004; p 497.

(15) Sorrentino, A.; Gorrasi, G.; Tortora, M.; Vittoria, V.; Constantino, U.; Marmottini, F.; Padella, F. *Polymer* **2005**, *46*, 1601–1608.

(16) Leroux, F.; Besse, J.-P. *Chem. Mater.* **2001**, *13*, 3507–3515.

(17) Palmer, S. J.; Frost, R. L.; Nguyen, T. *Coord. Chem. Rev.* **2009**, *253*, 250–267.

(18) Kwak, S.-Y.; Kriven, W. M.; Wallig, M. A.; Choy, J.-H. *Biomaterials* **2004**, *25*, 5995–6001.

(19) Choi, J.-H.; Kwak, S.-Y.; Jeong, Y.-J.; Park, J.-S. *Angew. Chem., Int. Ed.* **2000**, *39*, 4041–4045.

(20) Xu, Z. P.; Zeng, Q. H.; Lu, G. Q.; Yu, A. B. *Chem. Eng. Sci.* **2006**, *61*, 1027–1040.

(21) Uan, J.-Y.; Yu, B.-L.; Pan, X.-L. *Metall. Mater. Trans. A* **2008**, *39A*, 3233–3245.

(22) Zhang, F.; Sun, M.; Xu, S.; Zhao, L.; Zhang, B. *Chem. Eng. J.* **2008**, *141*362–367.

(23) Yi, J.-l.; Zhang, X.-m.; Chen, M.-a.; Gu, R. *Scr. Mater.* **2008**, *59*, 955–958.

(24) Zhang, F.; Zhao, L.; Chen, H.; Xu, S.; Evans, D. G.; Dan, X. *Angew. Chem., Int. Ed.* **2008**, *47*, 2466–2469.

(25) Zhang, W.; Buchheit, R. G. *Corrosion* **2002**, *58*, 591–600.

(26) Buchheit, R. G.; Guan, H. *J. Coat. Technol. Res.* **2004**, *1*, 277–290.

(27) Leggat, R. B.; Zhang, W.; Buchheit, R. G.; Taylor, S. R. *Corrosion* **2002**, *58*, 322–328.

(28) Leggat, R. B.; Taylor, S. A.; Taylor, S. R. *Colloids Surf. A* **2002**, *210*, 83–94.

(29) Buchheit, R. G.; Guan, H.; Mahajanam, S.; Wong, F. *Prog. Org. Coat.* **2003**, *47*, 174–182.

(30) Mahajanarn, S. P. V.; Buchheit, R. G. *Corrosion* **2008**, *64*, 230–240.

(31) Williams, G.; McMurray, H. N. *Electrochem. Solid-State Lett.* **2004**, *7*, B13–B15.

(32) Williams, G.; McMurray, H. N. *Electrochem. Solid-State Lett.* **2003**, *6*, B9–B11.

(33) Murray, H. N.; Williams, G. *Corrosion* **2004**, *60*, 219–228.

(34) Kendig, M.; Hon, M. *Electrochem. Solid-State Lett.* **2005**, *8*, B10–B11.

(35) Chico, B.; Simancas, J.; Veja, J. M.; Granizo, N.; Diaz, I.; Fuente, D.; Morcillo, M. *Prog. Org. Coat.* **2008**, *61*, 283–290.

(36) Yu, X.; Wang, J.; Zhang, M.; Yang, P.; Yang, L.; Cao, D.; Li, J. *Solid State Sci.* **2009**, *11*, 376–381.

(37) Theng, B. K. G. In *The Chemistry of Clay–Organic Reactions*; Theng, B. K. G., Ed.; Wiley: New York, 1974.

(38) Leroux, F.; Besse, J.-P. In *Clay Surfaces: Fundamentals and Applications*; Wypych, F., Satyanarayana, K. G., Eds.; Elsevier: London, 2004; pp 459–495.

(39) Zheludkevich, M. L.; Yasakau, K. A.; Poznyak, S. K.; Ferreira, M. G. S. *Corros. Sci.* **2005**, *47*, 3368–3383.

(40) Yang, H.; Sun, Y.; Ji, J.; Song, W.; Zhu, X.; Yao, Y.; Zhang, Z. *Corros. Sci.* **2008**, *50*, 3160–3167.

(41) Shchukin, D. G.; Lamaka, S. V.; Yasakau, K. A.; Zheludkevich, M. L.; Ferreira, M. G. S.; Möhwald, H. *J. Phys. Chem. C* **2008**, *112*, 958–964.

(42) Lamaka, S. V.; Zheludkevich, M. L.; Yasakau, K. A.; Montemor, M. F.; Ferreira, M. G. S. *Electrochim. Acta* **2007**, *52*, 7231–7247.

(43) Velu, S.; Ramkumar, V.; Narayanan, A.; Swamy, C. S. *J. Mater. Sci.* **1997**, *32*, 957–964.

(44) Bookin, A. S.; Drits, V. A. *Clays Clay Miner.* **1993**, *41*, 551–557.

(45) Bookin, A. S.; Cherkashin, V. I.; Drits, V. A. *Clays Clay Miner.* **1993**, *41*, 631–634.

(46) Kameda, T.; Yamazaki, T.; Yoshioka, T. *Microporous Mesoporous Mater.* **2008**, *114*, 410–415.

AM900495R